Soft Collisions of Highly Charged Ions with C_{60}

In slow collisions with complex targets, such as large atoms, clusters, and surfaces, highly charged ions may capture a large number of electrons into highly excited states, thereby leading to the temporary formation of unstable, multiply excited projectiles, commonly referred to as "hollow ions." Recent collision experiments with fullerene targets have made it possible to distinguish between close collisions that strongly favor fragmentation of the fullerene and distant collisions that primarily (multiply) ionize the fullerene. This Comment focuses on distant (soft) collisions of slow incident highly charged ions with gaseous C_{60} targets. It reviews a (mostly) classical model for multiple electron transfer and emission that simulates a variety of recently measured observables, such as electron capture cross sections, charge-state evolutions, projectile deflection angles, and projectile kinetic energy gains.

Keywords: *charge exchange, fullerenes, scattering, energy gain*

I. INTRODUCTION

The truncated icosahedral molecular structure of C_{60} and its large number of vibrational degrees of freedom make this highly symmetrical cluster with 240 valence electrons unusually stable.[1] The cage-structure of C_{60} was observed to withstand the reflection from a surface,[2] and photoionization and collision experiments with highly charged ions (HCI) have produced C_{60}^{q+} ions in positive charge states up to $q = 9$[3]

Comments At. Mol. Phys.
1999, Vol. 34, No. 3-6, pp. 119-140
Reprints available directly from the publisher
Photocopying permitted by license only

that do not dissociate for at least several microseconds. The relatively large thermal stability and huge polarizability make C_{60} an unusual and interesting target for collision studies in which it can be easily vaporized and serve as a gaseous target for incoming electrons, atoms, and ions. Highly charged ions, in particular, allow for the investigation of the dynamic electronic response of C_{60} clusters to a strong external perturbation that may lead to multiple capture and emission of electrons, and to (multiple) fragmentation. The analyses and theoretical modeling of such collisions constitute not only an important tool for examining the static and dynamic properties of fullerenes and their basic interaction mechanisms with highly charged projectile ions,[1,4–9] but also allow for the study of the complicated electronic dynamics involved in the collisional creation and post-collisional decay of unstable and multiply excited projectiles due to Auger electron and X-ray emission[3,10,11] (Fig. 1 and Table I).

TABLE I Time scales relevant for the formation and relaxation of hollow ions (of core charge q_{core}). Typical values for 80 keV Ar^{8+} interacting with C_{60}. The plasmon response time is estimated by $\sqrt{\frac{2\pi}{n_{el}}}$, where n_{el} is the average electron density of C_{60}

collision time for resonant exchange:	5 fs
orbiting time of first active projectile level (n = 7);	0.8 fs
plasmon response time of C_{60}:	0.2 fs
average time between successive electron capture events:	0.3 fs
projectile Auger transitions:	> 0.1 fs
projectile radiative transitions:	$q_{core}^{-4} \cdot 10^{-8}$ s

The interaction of a HCI with C_{60} is intermediate between an ion-atom collision and an ion-surface collision and displays certain features of ion-surface collisions in pure form. Similar to a surface, C_{60} provides a large reservoir of electrons. As for an insulating target surface, electron capture by a HCI results in a multiply charged target. The capture-induced target charges, in turn, influence the subsequent charge-transfer dynamics and the projectile trajectory. In contrast to

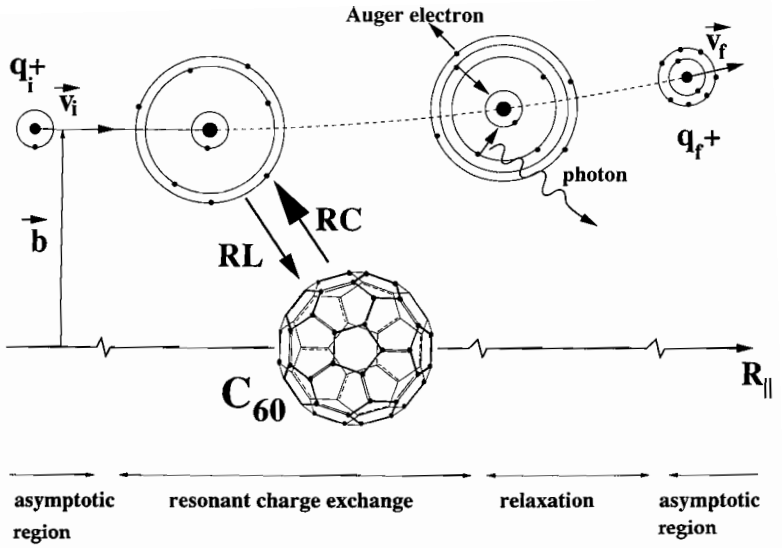

FIGURE 1 Sketch of the collisions scenario (not to scale). A highly charged ion with initial charge q_i, velocity $\mathbf{v}_i$, and impact parameter **b** carries a few (one) tightly bound electrons into the collision. At distances of the order of 10 to 100 a.u. from the target center it resonantly captures (RC) and (to a lesser extent) loses (RL) electrons. This leads to a positively charged target and a multiply excited, hollow projectile. Downstream and past the resonant interaction region, the unstable hollow projectile relaxes by emitting Auger electrons and X-rays, It may then be detected with final charge state q_f and velocity $\mathbf{v}_f$. The projection of the target-projectile distance R onto the incident-beam direction is denoted by $R_{||}$

HCI-surface collisions and as in ion-atom interactions, the collision geometry limits the interaction time with the cluster, allowing the projectile to avoid the nearly complete neutralization which usually accompanies its reflection from a surface.[12]

Collision experiments of HCIs with C_{60} are currently attracting increasing interest.[3,5,9,10] The experiments done by Walch *et al.*[6] probed the interaction between slow, highly charged ions and gaseous C_{60} targets and measured the final charge-states of target and projectile in coincidence. This coincidence measurement allowed for the distinction between hard collisions at relatively small impact parameters that lead to fragmentation of the target-carbon cage and non-destructive, soft collisions at larger impact parameters.

In this Comment, we focus on resonant electron exchange and the emission of projectile Auger electrons during and after soft collisions of a HCI with C_{60}. In Section II we give a brief overview of the dynamical classical over-barrier model (COM). Numerical results for charge-state evolutions and emitted electron yields follow in Section III. In the subsequent sections, the COM predictions for the following observables are discussed and compared with recent experiments: cross sections for the capture of a specific number of target electrons (Section IV), final projectile charge states (Section V), the projectile kinetic image energy gain (Section VI), and the projectile scattering angle (Section VII). Conclusions follow in Section VIII. Unless otherwise stated, atomic units are used throughout this Comment.

II. FORMATION OF HOLLOW IONS

Many features of the interaction between slow highly charged ions and complex atomic or molecular targets can be described by using classical model assumptions. In classical over-barrier models the electronic interaction with highly charged ions is modeled within the independent electron picture and is based on the effective potential to which an active electron, i.e., an electron that might be captured or lost, is subjected. An important feature of this effective potential is the potential barrier located between target and projectile. Position and height of the barrier change during the collision due to the relative motion and changing electronic structure of the collision partners. The over-barrier model allows for resonant transitions if the motion of a target or projectile electron across the potential barrier is classically possible, if the initial electronic state is at least partly occupied, and if the final state is not fully occupied in order to prevent Pauli blocking. In the past, various versions of over-barrier models have been successfully applied to slow collisions of ions with atoms,[13] surfaces,[14] and clusters.[6–8,11,15] The common attractive feature in these applications is that basic ideas of classical dynamics and electrostatics yield reasonable estimates for charge-transfer cross sections, charge-state distributions, and other observables that are beyond the technical feasibility of full quantum calculations.

During the ion-cluster interaction, energy levels, level occupations, transition rates, and total charges of target and projectile vary as a function of R, the distance between the centers-of-mass of target and projec-

tile. For the slow collisions considered in this Comment, R does not change on the time scale of resonant electronic transitions, and an adiabatic approximation is generally justified. In order to be captured or recaptured, the active electron is required to overcome the potential barrier V_B between target and projectile that is formed by the total electronic potential

$$V(q_p, q_t, R, z) = -\frac{q_p}{|R - z|} - \frac{q_t}{z} + V_{im}(q_p, R, z) \qquad (1)$$

where q_p and q_t are the charges of projectile and target acting on the electron in transition. The electron coordinate along the "inter-nuclear axis" is denoted by z. The image potential V_{im} includes the active electron's interaction with its self-image and with the image of the effective projectile charge q_p in the target. The barrier height V_B is found numerically for any distance R as the maximum of $V(q_p, q_t, R, z)$, considered as a function of z.

As the projectile approaches the target, the first resonant transfer of an electron becomes possible at the distance R_1^* between the projectile and target centers-of-mass, when V_B energetically moves below the highest occupied target level. Similarly, as R decreases, a second, third, etc. electron may be captured at critical distances $R_2^* > R_3^* \ldots$ on the incoming trajectory. Note that for the purpose of investigating electron capture mechanisms, the heavy projectile may be assumed to move along a straight-line trajectory (see Section VII for the experimental and computational verification of very small scattering angles of the order of a few mrad). The critical distances R_i^* are thus equal to critical impact parameters at which the trajectory becomes tangent to a sphere of radius R_i^* about the target center. Since the electronic charge is treated as a continuous parameter, some assumption has to be made as to when a complete electron has been transferred. Therefore, we define R_1^* as the impact parameter at which charge begins to flow from the target to the projectile, and R_2^* as the impact parameter at which one unit of charge has left the target, etc.

We describe the projectile within an independent electron approach based on hydrogenic shells n with energy levels, occupation numbers, and degeneracies denoted by $\epsilon_n^p(R)$, $a_n(R)$, and $A_n = 2n^2$, respectively. During the collision, the projectile energy levels shift due to image-charge effects, Stark shifts induced by a charged target, and the dynamical change in screening induced by varying level populations.

Target energy levels $\epsilon_m^t(R)$ are shifted downward in the electric field of the positive projectile. After the capture of target electrons, positive charge accumulates on the target, which results in an additional downward shift of the target and projectile spectra.

The time evolution of the occupations $a_n(t)$ and $b_m(t)$ of projectile shells n and target levels m are obtained by integrating classical rate equations of the form

$$\frac{d}{dt}a_n = \Gamma_{RN} - \Gamma_{RL}a_n + \sum_{n'>n} \Gamma_{n',n} - 2\sum_{n'<n} \Gamma_{n',n}, \qquad (2)$$

$$\frac{d}{dt}b_m = \Gamma_{RL}a_n - \Gamma_{RN}, \qquad (3)$$

by using the known initial occupations of projectile and target, a_n^0 and b_m^0. Analytical expressions for the resonant-capture rates Γ_{RN} and resonant-loss rates Γ_{RL} can be derived as classical transfer currents.[7,16] All rates and occupation numbers implicitly depend on $R(t)$, and the above equations are solved simultaneously with Newton's equation for the projectile motion. The two last terms of Eq. (2) include fast Auger transitions for which the two active electrons start in the same shell.[14] All rates implicitly depend on the level occupations a_n or b_m, such that Eqs. (2) and (3) together with the equation of motion for the projectile constitute a non-linear set of coupled differential equations that needs to be solved numerically. In particular, the resonant neutralization rate Γ_{RN} depends on the populations b_m of all target levels m that lie within a small interval* around the (shifted) energy of the resonant projectile level n. The Auger transition rates $\Gamma_{n1,n2}$ include statistical weights to take into account the number of electrons in the initial and final active shells. *Slow* Auger relaxation channels are not included, as they can be neglected *during* the collision (Table I). Further downstream, when resonant transfer processes are classically forbidden, Auger processes start to determine the final charge-state of the projectile. Downstream Auger and radiative relaxation steps can be accounted for by enhancing the dynamical COM with a simple relaxation scheme[11] (see Section V below).

The electronic structure of neutral C_{60} is well understood from first-principles calculations.[16–18] In applications to charge exchange and

* Within the dynamical COM, this "energy binning" is necessary in order to relate classical transfer currents to discrete quantum levels (Refs. 7 and 16).

electron emission in soft ion-C_{60} collisions, we employed a multi-center self-consistent Dirac-Fock-Slater (DFS) calculation[16,18] to obtain ground-state electronic structures of neutral C_{60} and its positive ions C_{60}^{i+}, $i = 0 \ldots 6$. This calculation yields the DFS single particle energies of C_{60}^{+i} for $i = 0 \ldots 7$ and the sequence of ionization potentials $I_{i=1 \ldots 7}$ = 7.24, 10.63, 14.01, 17.44, 20.78, 24.24, and 27.54 eV, in good agreement with other calculated and experimental data. Higher ionization potentials I_i, $i > 7$ can be approximated by taking into account the work necessary to remove an eighth, etc., electron from the surface of a conducting sphere of radius $a = 6.7$, $I_i = I_1 + (i - 1)/a$.[7] In agreement with a simple electrostatical model that represents the C_{60} cluster as a uniformly charged sphere, the incremental increase of ionization energies is due to the net charge of the cluster, and the sequence of ionization energies increases linearly with the net cluster charge q.

III. CHARGE-STATE EVOLUTION AND ELECTRON EMISSION

A detailed picture of the neutralization dynamics is given in Fig. 2, where changes in occupation numbers (i.e., the instantaneous occupation minus the initial occupation of a particular projectile level) are shown as a function of $R_{||}$, the projection of the distance between the target center-of-mass and the projectile onto the incident beam direction. The figure shows results for incident Ar^{8+} at a kinetic energy of 80 keV on a trajectory with impact parameter $b = 15$ (Fig. 2a) and Bi^{46+} at 800 keV with $b = 25$ (Fig. 2b). For the Ar^{8+} projectile, levels $n = 6$ and 7 get resonantly populated on the incoming trajectory ($R_{||} < 0$), in agreement with experimental evidence for capture into the $n = 7$ shell.[6,9] Auger relaxation of the projectile on the outgoing trajectory ($R_{||} > 0$) leads to the partial depletion of projectile levels $n = 6$ and 7 and increases the population in projectile levels $n = 3$ and 4.

A more extreme case of population inversion is achieved for the Bi^{46+} projectile. Figure 2b shows that resonant transitions first populate projectile shell $n = 31$ and, as the projectile further approaches the target, eventually lead to the population of shells with principal quantum numbers between 19 and 31. With respect to the target, the COM predicts a large current of resonantly captured electrons that originate in the large number of energetically densely spaced, occupied levels near the Fermi level of C_{60}.[16] In general, the large flux of captured electrons is accom-

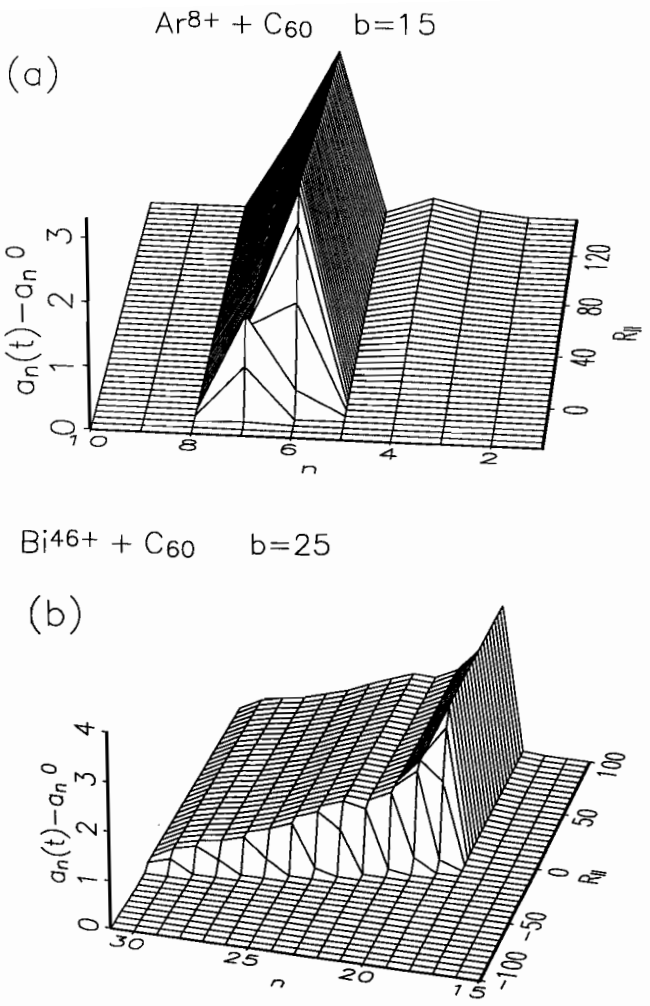

FIGURE 2 Evolution of projectile level occupations in collisions with C_{60}. The point of closest approach is at $R_{||} = 0$. (a) For incident 80 keV Ar^{8+} projectiles and impact parameter $b = 15$ a.u. (b) For 830 keV Bi^{46+} and $b = 25$ a.u. The graphs show the dynamical change $a_n(t) - a_n^0$ in the population of projectile shells $n = 1$ to $n = 31$. The initial shell population is denoted as a_n^0 . $a_n(t)$ is the population at the distance $R_{||}(t)$ (cf. Fig. 1)

panied by a very small flux of previously captured electrons that are lost to initially unoccupied target levels above the Fermi level. The charge-state evolutions in Fig. 3 follow directly from the time-dependent occupations in (2) and (3). For the short collision time interval of about 15 fs covered in Figs. 2a and 3, Auger transitions are too slow to significantly depopulate excited projectile levels within this region of resonant interactions (cf. Fig. 1). The displayed current of emitted Auger electrons and the increase of the net projectile charge on the displayed part of the outgoing trajectory are therefore very small.

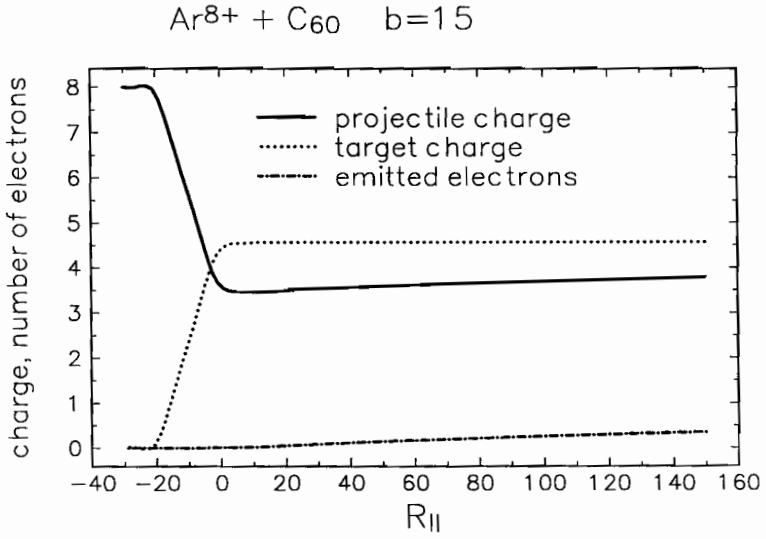

FIGURE 3 Projectile and target charge-state evolution and projectile Auger emission for incident 80 keV Ar^{8+} projectiles colliding with C_{60} at impact parameter $b = 15$ a.u.

Figure 4 shows the charge states of target and projectile as a function of the impact parameter and at $R_{||} = 150$ on the outgoing trajectory. At this distance all resonant electron transfer has stopped. Thus projectile Auger transitions had no time to relax the projectile. A lower limit for the impact-parameter range of non-destructive collisions is given by the highest charge state the target ions support without falling apart while interacting with the projectile. At the smallest impact parameter $b = 15$

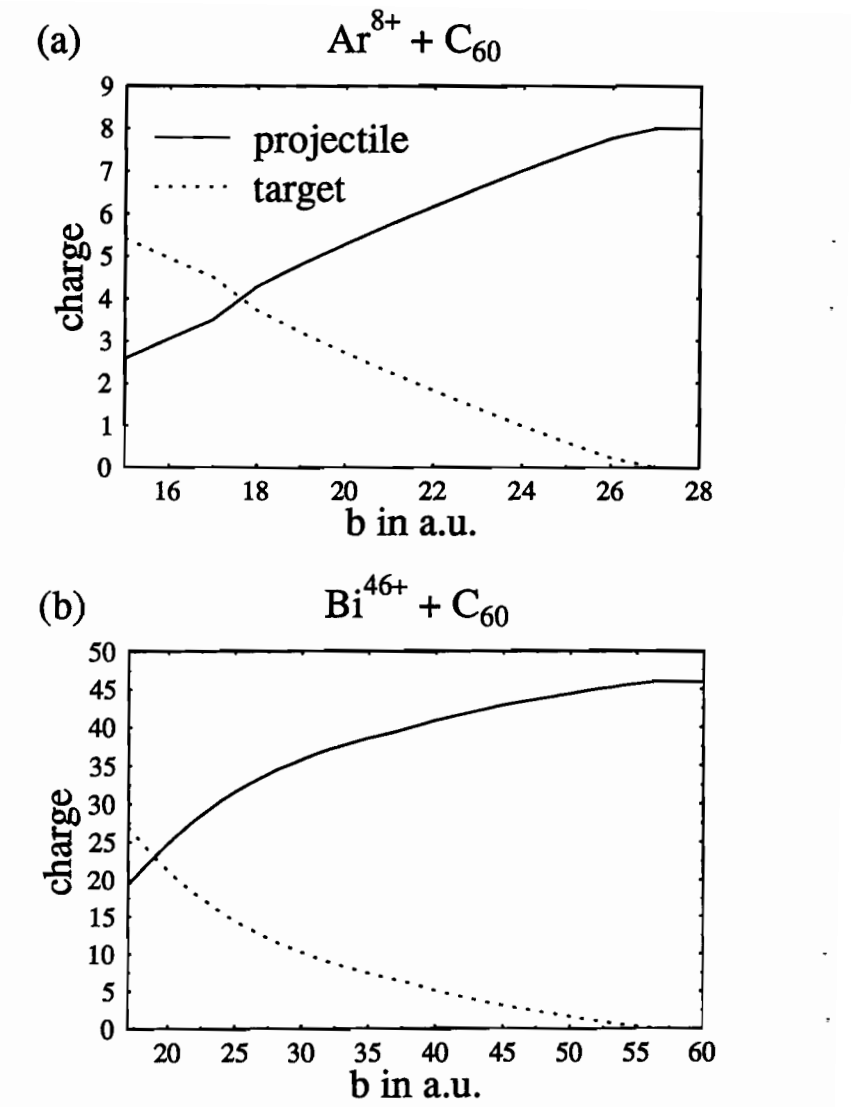

FIGURE 4 Projectile and target charge states as a function of the impact parameter b immediately after resonant electron exchange has ceased at $R_{||} = 150$ a.u. (a) For incident 26.4 keV Ar^{8+} projectiles. (b) For 830 keV Bi^{46+}

in Fig. 4a, the incident Ar^{8+} ion captures five electrons and thus maintains the carbon cage of the target.[6] At the smallest impact parameter in Fig. 4b, the incident Bi^{46+} has captured a large number of electrons and the target will certainly fall apart. In this case, the dynamical COM is applicable under the assumption that the multiply charged fullerene is stable *during* the collision, i.e., at least for several femtoseconds.

IV. CROSS-SECTIONS FOR MULTIPLE ELECTRON CAPTURE

As shown in Figs. 2 and 3 an HCI captures severals electrons on the incident trajectory. The sequence of critical radii R_i^* for the capture of i electrons can be extracted from the impact parameter dependence of the final target charge state shown in Fig. 4. Values for $3.3q$ keV Ar^{q+}, q = 8,15, are given in Table II. The critical distances R_i^* for sequential over-barrier capture are related to geometrical cross sections for the production of specific charge states, $+i$, of C_{60} by

$$\sigma_i = \pi(R_i^{*2} - R_{i+1}^{*2}) \tag{4}$$

and to the total geometrical cross section for charge exchange in non-destructive collisions by $\sigma_{tot} = \pi R_1^{*2}$. The cross sections in Table III are based on the critical radii in Table II. The calculated total cross sections agree with the absolute measurements performed by Walch *et al.*[6] and by Selberg *et al.*[9]

TABLE II Critical over-barrier radii R_i^* for the production of final target charge states $+i$ in $3.3q$ keV Ar^{q+}, q = 8,15, collisions with C_{60}

i	Ar^{8+}	Ar^{15+}
1	26.9	34.8
2	23.9	31.4
3	21.6	28.9
4	19.4	26.7
5	17.7	24.8
6	15.9	23.0

TABLE III Geometrical cross sections σ_i (in 10^{-15} cm^2) for the production of final target charge states $+i$ in 3.3q keV Ar^{q+}, q = 8,15, on C_{60} collisions. σ_{tot} and σ_{tot}^{exp} are the calculated (Ref. 20) and measured (Refs. 6 and 9) total cross sections for charge-state changing collisions. The projectile shell n into which capture primarily occurs is given in parenthesis

	Ar^{8+}	Ar^{15+}
σ_1 (n)	13.4 (7)	19.8 (12)
σ_2 (n)	9.2 (7)	13.3 (12)
σ_3 (n)	7.9 (7)	10.8 (11)
σ_4 (n)	5.6 (6)	8.6 (10)
σ_5 (n)	5.3 (6)	7.6 (10)
σ_{tot}	63.7	107
σ_{tot}^{exp}[9]	46 ± 14	100 ± 31
σ_{tot}^{exp}[6]	44 ± 18	

As expected, the simulated cross sections for incident 50 keV N^{5+} ions ($\sigma_{tot} = 4.3 \times 10^{-14}$ cm^2)[8] are smaller than for slow Ar^{8+} projectiles (6.2×10^{-14} cm^2).[7] For N^{5+} resonant capture of delocalized electrons does not lead to fragmentation of C_{60}, in contrast to experimental[6] and theoretical evidence for 80 keV Ar^{8+} impact. Thus capture-induced fragmentation appears to require a minimal interaction strength that is not reached for N^{5+} ions at 50 keV impact energy.

V. RELAXATION OF HOLLOW IONS

Hollow ions, that were created in ion-cluster collisions, decay during the typically several microseconds of flight time needed by the projectile to cover the macroscopic distance between the collision (resonant-exchange) region and detector (Fig. 1 and Table I). This downstream decay can be modeled as a sequence of autoionizing and radiative relaxation steps.[11] Typically the HCI starts to relax via a cascade of Auger transitions. During these transitions, lower lying levels are populated. Later, when the Auger relaxation cascade has populated lower-lying shells, radiative transitions might compete for subsequent

relaxation steps, as predicted by branching ratios (radiative versus non-radiative transition rates) which put increasing weight on radiative transitions between *inner* shells around a heavy nucleus. Radiative relaxation steps may then proceed along the "Yrast" line of maximal angular momentum of the active electron. This is supported by the statistical dominance of high angular momentum states, the dipole selection rule ($\Delta l = 1$), and the resonant population of high angular momentum states at large impact parameters.

Multiply excited projectiles such as those generated in the case of incident Bi^{46+} ions (Fig. 2b) offer a large number of autoionizing transitions between the very many excited states of the hollow ion. These transitions can be combined to an even larger number of possible relaxation cascades such that a rigorous theoretical treatment of the relaxation process is currently out of reach. Therefore, we employed a simple relaxation scheme[11] based on intuition, basic features of emitted electron spectra, and wavefunction overlap arguments. This scheme is put together by prioritizing possible relaxation steps. It does not rely on transition rates. For any configuration of the relaxing ion, the most likely next (Auger or radiative) transition is assumed to happen instantaneously and with unit probability. The relaxation can be summarized as follows:

a. Since Auger transitions are driven by electron-electron correlation in the initial state, the relaxation cascade is assumed to start with transitions that (i) involve electrons in the outermost occupied shell(s) of the hollow ion and (ii) minimize the kinetic energy of the emitted electrons. This agrees with the general observation of very strongly enhanced emitted electron energy spectra close to the continuum threshold, as well as with a relatively large wavefunction overlap between initial and final state. Our relaxation scheme gives highest priority to active electron pairs in identical or adjacent outer shells. Among these pairs, those favored include the most highly excited outer electron. Next on the priority list are transitions with the smallest possible change in principal quantum number of the inner electron that still lead to emission. This pattern is repeated until the ion is stable with respect to Auger decay.

b. Radiative transitions may continue to relax the excited ion. Radiative transition probabilities are largest for the lowest lying final states and, among those, for the lowest emitted photon energies.[19]

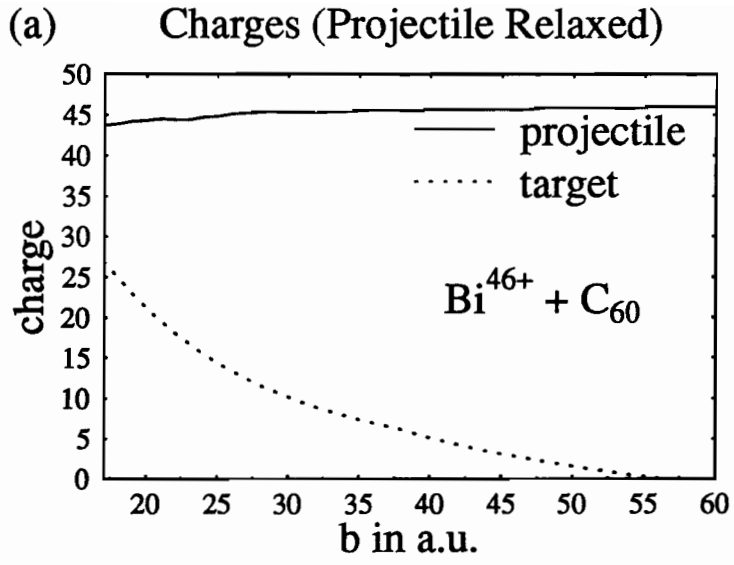
(a)
Charges (Projectile Relaxed)
charge
b in a.u.
projectile
target
$Bi^{46+} + C_{60}$

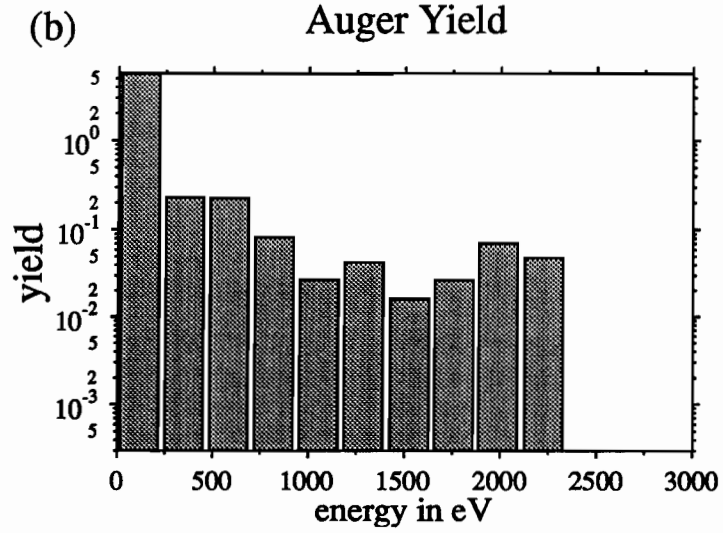
(b)
Auger Yield
yield
energy in eV

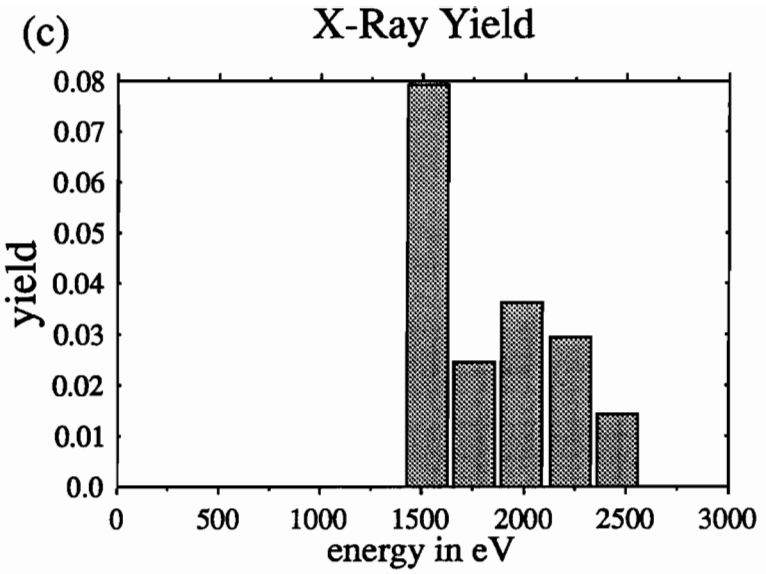

FIGURE 5 Results for 830 keV Bi^{46+} colliding with C_{60}, including downstream projectile relaxation. (a) Projectile and target charge states as a function of the impact parameter *b*. (b) Simulated Auger electron yield. (c) Simulated X-ray yield

Thus we first allow for radiative transitions into vacancies in the lowest shells with at least one vacancy and repeat this scheme until all inner vacancies are filled.

Figure 5 shows results for incident 830 keV Bi^{46+} ions, including the downstream relaxation of the projectile. As a consequence of the downstream relaxation process, most of the captured electrons get autoionized, as is easily seen by comparing Fig. 5a with Fig. 4b. The incident projectile charge effectively changes by no more than a few units. As suggested by a simple order-of-magnitude comparison of the collision time and typical Auger transition times (cf. Table I), autoionization is practically restricted to deexcitations that happen after the collision (cf. Fig. 3). The simulated yields of emitted Auger electrons and X-rays in Figs. 5b and 5c are accumulated over 234 eV wide intervals of emitted electron and photon energies, respectively. They are normalized to the area perpendicular to the incident beam direction that intersects projec-

tiles with impact parameters between $b_{min} = 17$ and $R_1^* = 57.0$. For these collisions, the total X-ray yield divided by total Auger yield amounts to 0.03.

VI. PROJECTILE KINETIC ENERGY GAIN

The change in the balance between potential and kinetic energy of the collision system can be obtained by integrating the net force between target and projectile along the trajectory. In the center-of-mass frame of reference, this amounts to integrating the force that governs the motion of the projectile of reduced mass along its trajectory. It defines the "*nuclear*" *energy defect* Q_{nuc},[20] which is directly related to the motion of the reduced-mass projectile considered as a structure-less particle of variable charge. The net force is the sum of the direct Coulomb and image charge interactions between target and projectile and is provided as a function of time within the dynamical COM.

Due to energy conservation, Q_{nuc} is identical to the difference of the total electronic binding energy of the collision system before and after the collision. This "*electronic*" *energy defect* is denoted by Q_{el}.[20] Since our simulation includes approximations to the complex dynamics of the multi-particle collision system that affect the coupling between nuclear and electronic degrees of freedom, we expect our calculated values for Q_{el} and Q_{nuc} to differ. The difference $|Q_{nuc} - Q_{el}|$ is related to the accuracy of the simulated translational energy gains. The electronic and nuclear energy defects for incident 46.2 keV Ar^{14+} ions are compared in Fig. 6. The structure in Q_{el} is due to binning effects (i.e., it is related to the assignment of classical energy intervals to discrete quantum levels within the COM[20]), and the two defects agree within the overall accuracy of the COM.

In order to compare theory with measured projectile energy-gain spectra, we relate the critical radii for the sequential capture of electrons to energy defect values and to the number of electrons that are captured for a particular impact parameter (cf. Figs. 4 and 6). For impact parameters $b_i = R_{i+1}^*$, i electrons have been captured, and the corresponding energy defects are $Q_{nuc}(b_i)$ and $Q_{el}(b_i)$. The simulated, discrete energy defects are folded with a Gaussian distribution R in order to correct for the finite experimental energy resolution. The full width at half maxi-

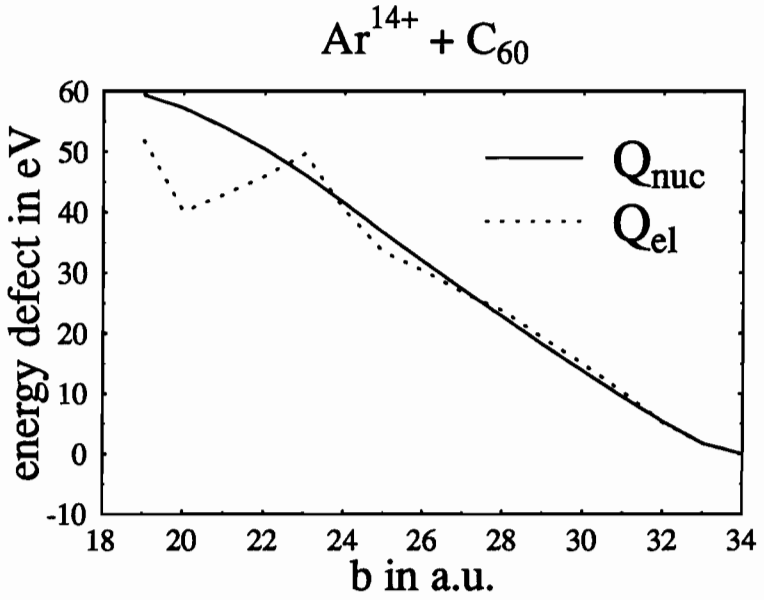

FIGURE 6 Electronic and nuclear energy defects as a function of the impact parameter b, converged at a distance of $R_{||}$=50000 a.u. downstream, for Ar^{14+} colliding with C_{60} at 46.2 keV

mum of R is adjusted to the resolution of the experiment. The simulated energy gain spectrum is now given by the cross section

$$\frac{d\sigma}{d\Delta E} = \sum_i \sigma_i R(\Delta E - Q_i) \tag{5}$$

which is differential in the projectile kinetic energy gain ΔE.

This method allows for the interpretation of peaks in the measured spectra in terms of the corresponding number of captured electrons. In conjunction with the simulated projectile occupation changes (cf. Fig. 2) it also allows for the assignment of final projectile shells into which capture occurs at particular energy gains. Figure 7 shows a measured differential energy gain spectrum from Selberg *et al.*[8] together with the simulated spectra for the removal of a specific number of electrons from C_{60}.[20] Experimental and calculated spectra are absolute, both in

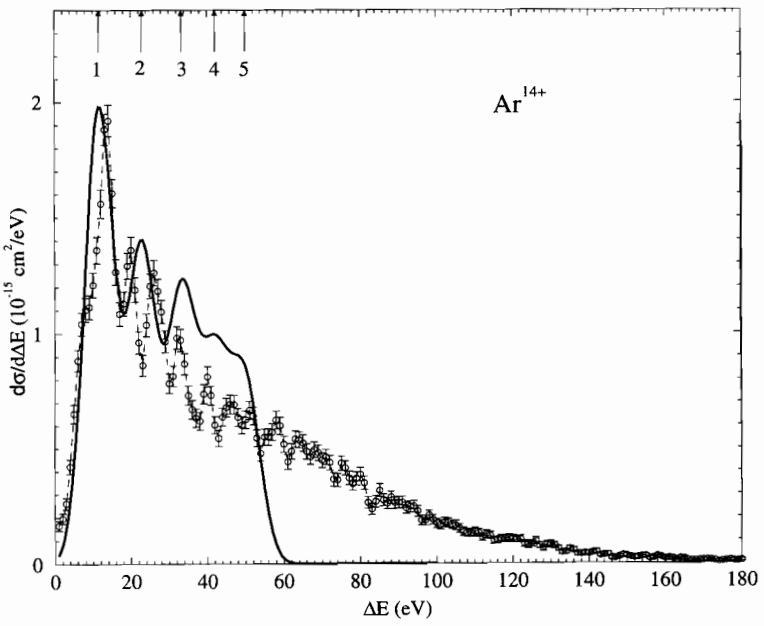

FIGURE 7 Simulated and measured projectile energy gain spectra for 46.2 keV Ar^{14+}-C_{60} collisions. The measured and calculated energy gain values and peak heights (cross sections) are absolute. The experimental errors in peak positions are typically ±0.5 eV. The arrows point to the calculated nuclear energy defects for the capture of 1, 2, 3, etc., electrons

intensity (peak heights) and energy gain. Calculated energy gains correspond to the nuclear defects and include the five lowest energy gains. In the overall trend, the lower part of the measured spectrum, which yields the dominant contribution to the total cross section, agrees well with the simulation. The calculated nuclear energy defects are indicated by numbered arrows and correspond to capture into specific projectile shells (1: capture into $n = 12$, 2: into $n = 11$, 3: into $n = 11$, 4: into $n = 10$, 5: into $n = 10$). The high energy gain region cannot be explained by the present dynamical COM, and further investigations are necessary to fully understand this part of the kinetic energy gain spectrum. Similarly, even though reproducing the main features of the low-energy part of measured energy gain spectra on an absolute scale, the COM needs further

refinement in order to more accurately reproduce measured gains, e.g., for the capture of two electrons in Fig. 7. A rewarding step in this direction could be the inclusion of projectile sub-shells *nl* which are not resolved within the current version of the COM.

VII. TARGET DIELECTRIC RESPONSE AND PROJECTILE ANGULAR DISTRIBUTIONS

Due to the large polarizability of C_{60}, the trajectory of a highly charged ion capturing electrons in the "soft" over-barrier region of impact parameters is affected measurably by the polarization potential between projectile and target. This effect is a truncated analog of the image charge acceleration for highly charged ions incident on solid surfaces.

Simulations for slow incident highly charged ions colliding with C_{60} have predicted[8,16] that the deflection function, i.e., the projectile scattering angle as a function of impact parameter, is characterized in its overall trend by two broad extrema that originate in the competition between attractive induced polarization and repulsive Coulomb interactions between (charged) target and projectile. These maxima lead to strong enhancements in the angle-differential scattering cross section, usually referred to as "Rainbow-Scattering."

An experimental angle resolution of ≈ 0.01 degrees pointed to a potentially measurable prominent structure in the angle-differential cross section. Walch *et al.*[21] have measured the angular distributions of 2.5 keV Ar^{8+} projectiles following the capture of 1 to 5 electrons from C_{60}. Their angular distributions (Fig. 8) show a strong increase of deflection angle with the number of electrons removed from C_{60}, due to the increasing Coulomb repulsion between positively charged collision partners. The simulated angular distributions, including the attractive self-interaction of the projectile with the dipole it induces in the target, are shown in Fig. 8 as solid lines. The same simulations, however without the induced polarization effects, are shown as dotted lines. The agreement between the COM simulation and experiment in the location of the maxima is remarkable, showing that the model describes the basic interaction very well, even to the detail of the angular distributions. The effect of the induced target polarization on the deflection of the projectile is clearly observed in all cases shown.

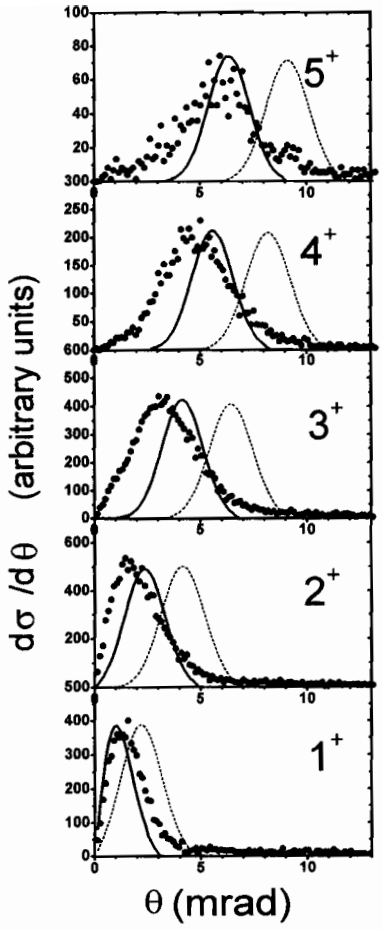

FIGURE 8 Angular distributions for the capture of $i = 1 \ldots 5$ electrons from C_{60} by 2.5 keV Ar^{8+} ions. Each figure is labeled by $i+$, θ is the deflection angle. The solid curves are the COM calculations including target polarization. The dashed curves are calculated without this polarization

VIII. CONCLUSIONS

The dynamical COM simulates the formation of hollow ions during the interaction of slow, highly charged ions with C_{60}. This Comment has put together several applications of the dynamical COM to observables that recently have been measured in this new type of heavy-ion collision. Furthermore, it has analyzed the downstream relaxation of collisionally produced hollow ions within a simple relaxation scheme which allows for the simulation of energy differential and total yields of post-collisionally emitted projectile Auger electrons and photons.

Future investigations, both experimental and theoretical, are necessary to refine these simulations in order to better understand the exciting life of a hollow ion during and after its interaction with a many-electron target, such as C_{60}. In particular, the COM may be improved by including more accurate polarizabilities of C_{60} and its positive ions and by a realistic modeling of the finite conductivity of C_{60}. The polarizabilities are expected to influence angular distributions in very slow collisions.[21] The careful study of localization and mobility of capture-induced positive charge on C_{60}[22] is of interest to the new field of fullerene chemistry in possibly helping us to better understand the formation of chemical bonds with fullerenes[23] and may point to dominant fragmentation mechanisms of charged fullerenes.[24]

Acknowledgments

Many stimulating discussion and the collaboration with A. Bárány, H. Cederquist, C. L. Cocke, B. Fricke, L. Hägg, C. J. Setterlind, and B. Walch are gratefully acknowledged. This work was supported by the Division of Chemical Sciences, Office of Basic Energy Sciences, Office of Energy Research, U.S. Department of Energy, NFS, and by the Kansas Center for Advanced Scientific Computing sponsored by the NSF/K*STAR program.

UWE THUMM
J. R. Macdonald Laboratory,
Department of Physics,
Kansas State University,
Manhattan, Kansas 66506–2604, USA

References

1. D.C. Lorentz, Comments At. Mol. Phys. **33,** 125 (1997).
2. H.G. Busmann, Th. Lill, B. Reif and I.V. Hertel, Surf. Sci. **272**, 146 (1992).
3. J. Jin, H. Khemliche, M.H. Prior and Z. Xie, Phys. Rev. A **53,** 615 (1996).
4. P. Hvelplund, L.H. Anderson, H.K. Haugen, J.Lindhard, D.C. Lorents, R. Malhotra and R. Ruoff, Phys. Rev. Lett. **69,** 1915 (1992).
5. T. LeBrun, H.G. Berry, S.Cheng, R.W. Dunford, H.Esbensen, D.S. Gemmel and E.P. Kanter, Phys. Rev. Lett. **72,** 3965 (1994).
6. B. Walch, C.L. Cocke, R. Voelpel and E. Salzborn, Phys. Rev. Lett. **72,** 1439 (1994).
7. U. Thumm, J. Phys. B **27,** 3515 (1994).
8. U. Thumm, J. Phys. B **28,** 91 (1995).
9. N. Selberg, A. Bárány, C. Biedermann, C.J. Setterlind, H. Cederquist, A. Langereis, M.O. Larsson, A. Wännström and P. Hvelplund, Phys. Rev. A **53,** 874 (1996).
10. J.P. Briand, L. de Billy, J. Jin, H. Khemliche, M.H. Prior, Z. Xie, M. Nectoux and D. Schneider, Phys. Rev. A **53,** R2925 (1996).
11. U. Thumm, Phys. Rev. A **55,** 479 (1997).
12. S. Winecki, C.L. Cocke, D. Fry and M.P. Stöckli, Phys. Rev. A **53,** 4228 (1996).
13. A. Bárány, G. Astner, H. Cederquist, H. Danared, S. Huldt, P. Hvelplund, A. Johnson, H. Knudsen, L. Liljeby and K.-G. Rensfeld, Nucl. Instrum. Methods Phys. Res. B **9,** 397 (1985); A. Niehaus, J. Phys. B **19,** 2925 (1986).
14. J. Burgdörfer, in *Review of Fundamental Processes and Applications of Atoms and Ions,* edited by C. D. Lin (World Scientific, Singapore, 1993), p. 517.
15. A. Bárány and C.J. Setterlind, Nucl. Instrum. Methods Phys. Res. B **98,** 184 (1995).
16. U. Thumm, T. Baştuğ and B. Fricke, Phys. Rev. A **52,** 2955 (1995).
17. C. Yannouleas and U. Landman, Chem. Phys. Lett. **217,** 175 (1994); J.L. Martins, N. Troullier and J.H. Weaver, ibid. **180**, 457 (1991).
18. T. Bastuğ, P. Kürpick, J. Meyer, W.-D. Sepp, B. Fricke and A. Rosen, Phys. Rev. B **55,** 5015 (1997).
19. E.U. Condon and G.H. Shortley, *The Theory of Atomic Spectra* (Cambridge University Press, 1957), pp. 136, 148.
20. U. Thumm, A. Bárány, H. Cederquist, L. Hägg and C.J. Setterlind, Phys. Rev. A **56,** 4799 (1997).
21. B. Walch, U. Thumm, M. Stöckli and C.L. Cocke, in *Abstracts of Contributed Papers, XX International Conference on the Physics of Electronic and Atomic Collisions,* ed. F. Aumayr G. Betz and HP. Winter, p. FR086, Vienna, 1997.
22. H. Shen, P. Hvelplund, D. Mathur, A, Bárány, H. Cederquist, N. Selberg and D.C. Lorentz, Phys. Rev. A **52,** 3847 (1995).
23. S. Petrie, J. Wang and D.K. Bohme, Chem. Phys. Letters **204,** 473 (1993).
24. P. Scheier, B. Dünser and T.D. Märk, J. Chem. Phys. **99**, 15428 (1995).